Magic Electron Counts for Networks of Condensed Clusters: Vertex-Sharing Aluminum Octahedra

Grigori V. Vajenine and Roald Hoffmann*

Contribution from the Department of Chemistry, Cornell University, Ithaca New York 14853-1301

Received December 5, 1997. Revised Manuscript Received March 3, 1998

Abstract: The aluminum substructure of the AeM_2Al_9 (Ae = Ba and M = Fe, Co, Ni; Ae = Sr and M = Co, Ni; Ae = Ca and M = Co) and $CaNiAl_9$ compounds is a beautiful three-dimensional network of vertex-sharing aluminum octahedra. Bonding in this network is analyzed at the extended Hückel level by studying the effect of vertex sharing between isolated aluminum octahedral clusters in several model systems: a linear dimer of two clusters, a linear one-dimensional chain of clusters, a two-dimensional square sheet, and a three-dimensional cubic network of clusters. We find that the number of skeletal electrons per aluminum cluster optimal for Al−Al bonding is reduced from 14 for an isolated cluster to 12 for the cluster dimer and cluster chain, 10 for the two-dimensional cluster sheet, and 8 for the cubic network in which all cluster vertices are shared. Two effects are responsible for the reduction in the optimum electron count: First, vertex-sharing reduces the number of skeletal bonding orbitals per cluster (through restrictions due to translational symmetry in extended structures). Second, the levels just above the skeletal bonding states become Al−Al antibonding due to next-nearest-neighbor intercluster interactions. According to our calculations, Al−Al bonding in the aluminum network of the $BaFe_2Al_9$-type compounds is maximized for approximately 9 skeletal electrons per aluminum octahedral cluster, which is qualitatively consistent with the results obtained for the model systems and our assignment of formal charges. Connections are made to a number of related structures containing networks of main group octahedra.

Introduction

The common feature of the AeM_2Al_9 (Ae = Ba and M = Fe, Co, Ni; Ae = Sr and M = Co, Ni; Ae = Ca and M = Co)[1−3] and $CaNiAl_9$[1,4] phases is a beautiful network of aluminum atoms. Two views of the $BaFe_2Al_9$ structure are shown in Figure 1: one along the *c* axis of the hexagonal network and the other perpendicular to the *c* axis. The aluminum substructure may be described as a three-dimensional array of vertex-sharing Al_6 octahedra. These octahedra form a Kagomé net in the *ab* plane, as seen in Figure 1a. The octahedra are very close to being regular: the Al−Al nearest neighbor distances range from 2.85 to 2.98 Å, with the average of 2.89 Å. The Al−Al bond lengths parallel to the *ab* plane are a bit longer than the other Al−Al contacts, this difference ranging from 0.05 to 0.11 Å. Thus the octahedra are very slightly compressed along the *c* axis. The observed Al−Al bond lengths are similar to that in elemental aluminum (2.86 Å)[5] and in Laves phases such as $CaAl_2$ (2.83 Å).[6] The alkaline-earth atoms reside in the hexagonal channels, while the transition-metal atoms fill the trigonal channels of the network. The structure of $CaNiAl_9$ has every other transition-metal site empty compared to the $BaFe_2Al_9$ structure, the aluminum network being essentially the same. As the focus of this analysis will be on the fascinating aluminum substructure, a discussion of the bonding at alkaline-earth and transition-metal atoms is given in the Appendix.

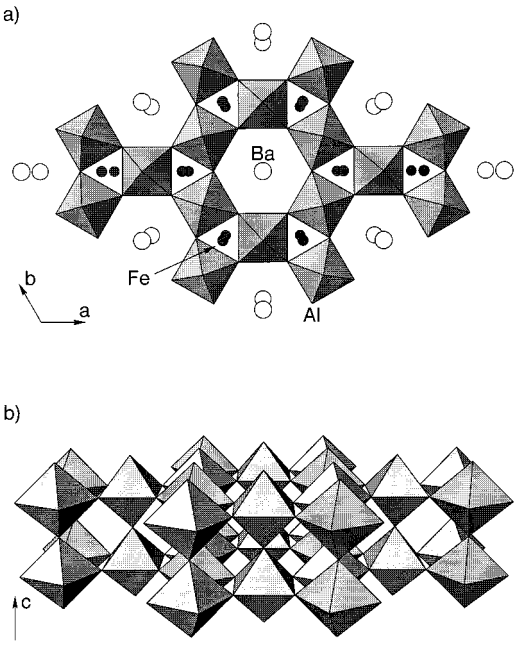

Figure 1. The $BaFe_2Al_9$ crystal structure viewed along the *c* axis. Vertex-sharing aluminum octahedra are emphasized (a). The octahedra of the aluminum network also share vertices along the *c* axis (b).

In our quest to relate complex extended systems to simpler molecular ones, we see in these structures the possibility of making a connection between the electronic structure of the aluminum network and bonding in an isolated aluminum

(1) Manyako, N. B.; Yanson, T. I.; Zarechnyuk, O. S. *Izv. Akad. Nauk SSSR, Met.* **1988**, 185.
(2) Turban, K.; Schäfer, H. *J. Less*-Common Met. **1975**, *40*, 91.
(3) Ainutdinov, F. A.; Khairidinov, S. Kh.; Vakhobov, A. V. *Dokl. Akad. Nauk Tadzh. SSR* **1987**, *30*, 169.
(4) Manyako, N. B.; Zarechnyuk, O. S.; Yanson, T. I. *Kristallografiya* **1987**, *32*, 1389.
(5) Otte, H. M.; Montague, W. G.; Welch, D. O. *J. Appl. Phys.* **1963**, *34*, 3149.
(6) Iandelli, A. *J. Less-Common Met.* **1987**, *135*, 195.

S0002-7863(97)04132-2 CCC: $15.00
Published on Web 04/18/1998

octahedral cluster. The bonding in the latter in turn is expected to be similar to that in the well-understood octahedral borane, $B_6H_6^{2-}$.

We begin our analysis with electron counting in the real alkaline-earth−transition-metal−aluminum intermetallics. We then discuss bonding in an octahedral Al_6H_6 cluster and study the effect of sharing a vertex between two such clusters in the following model systems: a linear cluster dimer, a linear one-dimensional chain of vertex-sharing clusters, a square two-dimensional sheet, and, finally, a cubic three-dimensional network of vertex-sharing clusters. In the end, we apply the knowledge thus obtained to the aluminum substructure of the above-mentioned intermetallics.

Extended Hückel Calculations

All electronic structure calculations were carried out using the extended Hückel method,[7−9] an approximate molecular orbital scheme, implemented with the YAeHMOP program.[10] The following parameters (energies and orbital exponents) were used for the Slater-type wave functions representing valence subshells of aluminum and hydrogen atoms: Al 3*s* $H_{ii} = -12.3$ eV, $\zeta = 1.167$; Al 3p $H_{ii} = -6.5$ eV, $\zeta = 1.167$; H 1s $H_{ii} = -13.6$ eV, $\zeta = 1.3$. The aluminum[11] and hydrogen[8] parameters were taken from previous work. The off-diagonal Hamiltonian matrix elements were computed with the modified Wolfsberg−Helmholtz formula.[12] *K*-point sets for average properties calculations were obtained according to Ramírez and Böhm.[13,14] As the compression of aluminum octahedra observed in the $BaFe_2Al_9$-type compounds does not significantly alter the computed electronic structure of the network, we use the idealized octahedral geometry in this study.

Electron Counting

Before addressing the bonding in the aluminum substructure of Figure 1, we attempt to assign formal charges to all elements forming the intermetallics. The electronegativities according to the Pauling scale[15] are as follows: 1.00−0.89 for Ca−Ba, 1.61 for Al, and 1.82−1.91 for Fe−Ni. The alkaline-earth atoms, being the most electropositive ones, are treated as divalent cations. The transition-metal atoms are, on the other hand, the most electronegative elements in this structure; note that this is an essential difference from typical binary or ternary Zintl compounds. At least as measured by the electronegativity differences, the transition-metal atoms are likely to accept electrons from the alkaline earths and aluminum. We are aware that proper inclusion of electron−electron repulsions and exchange may affect this supposition. A reasonable assumption is that a transition-metal atom will try to fill its 3d block of orbitals, resulting in a formal charge of −2 for iron, −1 for cobalt, and zero for nickel. Of course, this is just a convenient formalism; the real charges on the atoms will certainly differ from the assigned formal ones. What such a formalism allows us to do is to assign in a preliminary way the number of electrons available for Al−Al bonding in the aluminum substructure. The resulting formal charges are as follows: $Ba^{2+}(Fe^{2-})_2(Al_9)^{2+}$, $Ba^{2+}(Co^{-})_2(Al_9)^{0}$, $Ba^{2+}(Ni^{0})_2(Al_9)^{2-}$, $Sr^{2+}(Co^{-})_2(Al_9)^{0}$, $Sr^{2+}(Ni^{0})_2(Al_9)^{2-}$, $Ca^{2+}(Co^{-})_2(Al_9)^{0}$, and $Ca^{2+}Ni^{0}(Al_9)^{2-}$. Our calculations, in the end, emerge consistent with the $3d^{10}$ configuration for the transition-metal atoms in these compounds.

There are, therefore, 25−29 valence electrons per nine aluminum atoms. Every octahedral vertex is shared by two aluminum octahedra; thus, there is one Al_6 cluster per every three aluminum atoms. Every such cluster then has between $8^1/_3$ and $9^2/_3$ electrons for bonding. It is important to note that even if our formal procedure (electron transfer to M to complete the 3d block) is doubted, the number of electrons per aluminum cluster has to be in the vicinity of nine due to overwhelming dominance of aluminum in these intermetallics.

In the next section, we take a seemingly large step back and consider bonding in what can be viewed as the building block of the intermetallics—an isolated octahedral aluminum cluster.

Bonding in an Isolated Al_6H_6 Octahedron

The bonding picture for an octahedral Al_6 cluster is quite similar to that of the octahedral borane, $B_6H_6^{2-}$. The electronic structure of the latter and similar to it compounds has been addressed previously.[7,16−18] Bonding in the related gallium[19] and thallium[20] octahedral clusters has also been studied. We choose to "passivate" the aluminum atoms with hydrogens, so that the resulting Al_6H_6 cluster (Scheme 1) bears even more resemblance to its boron analogue. Such a model choice simplifies the analysis of the cluster bonding without altering the conclusions. The Al−Al distance was set at 2.89 Å, as observed experimentally in the intermetallics. The Al−H bond length was fixed at 1.55 Å, as in $LiAlH_4$.[21]

An AlH unit will be used as a building block for the cluster. The frontier orbitals of AlH are shown Scheme 2. There are two electrons in the single Al−H bond. For neutral AlH, the remaining two aluminum electrons are placed in the delocalized combinations arising from three local orbitals: one of which is traditionally labeled "radial", opposite to the Al−H bond, and two which are termed "tangential". The former orbital is a

Scheme 1

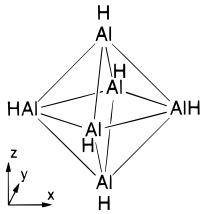

Scheme 2

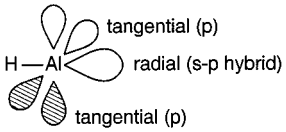

(7) Hoffmann, R.; Lipscomb, W. N. *J. Chem. Phys.* **1962**, *36*, 2179.
(8) Hoffmann, R. *J. Chem. Phys.* **1963**, *39*, 1397.
(9) Hoffmann, R. *Solids and Surfaces: A Chemist's View of Bonding in Extended Structures;* VCH: New York, 1988.
(10) Landrum, G. A. *Yet Another Extended Hückel Molecular Orbital Package (YAeHMOP)*; Cornell University, 1997. YAeHMOP is freely available on the World Wide Web at the following address: http://overlap.chem.cornell.edu:8080/yaehmop.html.
(11) Anderson, A. B.; Hoffmann, R. *J. Chem. Phys.* **1974**, *60*, 4271.
(12) Ammeter, J. H.; Bürgi, H.-B.; Thibeault, J. C.; Hoffmann, R. *J. Am. Chem. Soc.* **1978**, *100*, 3686.
(13) Ramírez, R.; Böhm, M. C. *Int. J. Quant. Chem.* **1986**, *30*, 391.
(14) Ramírez, R.; Böhm, M. C. *Int. J. Quant. Chem.* **1988**, *34*, 571.
(15) Huheey, J. E. *Inorganic Chemistry;* Harper & Row: New York, 1983.
(16) Longuet-Higgins, H. C.; Roberts, M. de V. *Proc. R. Soc. London A* **1954**, *224*, 336.
(17) Lipscomb, W. N. *Boron Hydrides;* W. A. Benjamin: New York, 1963.
(18) Mingos, D. M. P.; Wales, D. J. *Introduction to Cluster Chemistry;* Prentice Hall: Englewood Cliffs, NJ, 1990.
(19) Liu, Q.; Hoffmann, R.; Corbett, J. D. *J. Phys. Chem.* **1994**, *98*, 9360.
(20) Dong, Z.; Corbett, J. D. *J. Am. Chem. Soc.* **1993**, *115*, 11299.
(21) Greenwood, N. N.; Earnshaw, A. *Chemistry of the Elements*; Pergamon Press: New York, 1989; p 258.

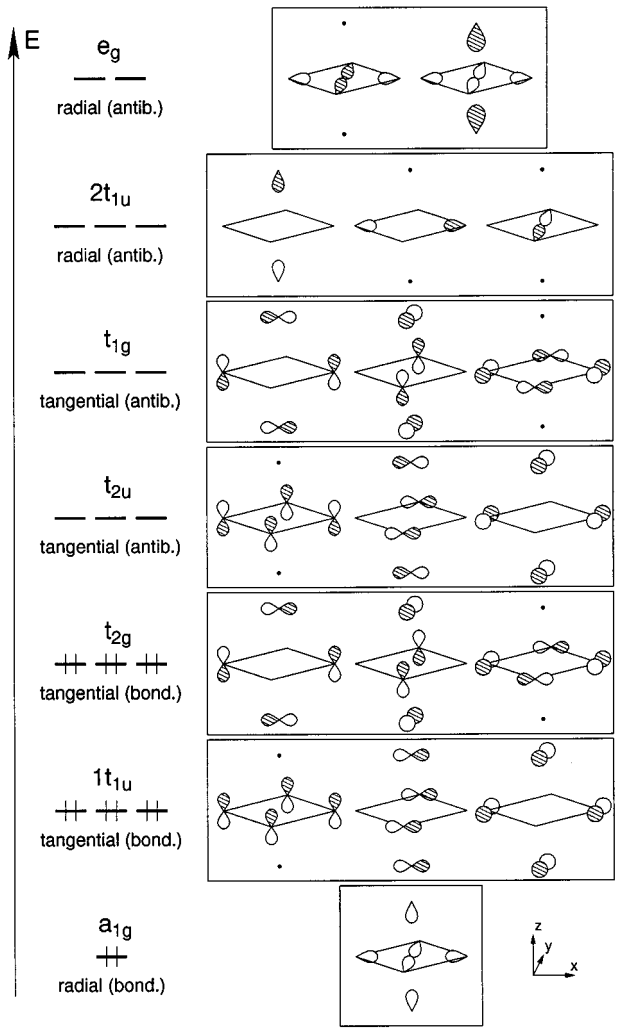

Figure 2. Cluster molecular orbitals in $Al_6H_6^{2-}$. The orbitals are qualitatively arranged on the energy scale.

hybrid between Al s and p orbitals, the latter two are pure Al p. The terms "radial" and "tangential" refer to the role these orbitals play as a cluster is assembled.

Six such AlH fragments are brought together to form an Al_6H_6 octahedron. The resulting molecular orbitals important for Al−Al bonding are shown in the *schematic* Figure 2 (the vertical scale is approximate). The six radial orbitals of the AlH fragments split into the following sets of orbitals: a_{1g}, t_{1u}, and e_g. The former is Al−Al bonding, the latter two sets are Al−Al antibonding (the t_{1u} orbitals are labeled $2t_{1u}$ in Figure 2). The 12 tangential orbitals form four triply degenerate sets of orbitals: Al−Al bonding ($1t_{1u}$ and t_{2g}) and Al−Al antibonding (t_{2u} and t_{1g}). This simple picture is somewhat complicated by mixing in of the six filled Al−H σ -bonding orbitals, which transform as a_{1g}, t_{1u}, and e_g—just the same symmetries as the six radial orbitals. The six Al−H σ-antibonding orbitals, which again belong to the same irreducible representations, also mix in, though to a much smaller extent. The other complication arises from mixing of the two cluster t_{1u} orbital sets: $1t_{1u}$ (tangential bonding) and $2t_{1u}$ (radial antibonding).

Despite these secondary interactions, the simple bonding picture for the octahedral Al_6H_6 cluster is still a good one. Filling up the lower seven Al−Al orbitals maximizes Al−Al bonding and results in a −2 charge on the cluster, with a sizable HOMO(t_{2g})−LUMO(t_{2u}) gap of 4 eV, according to our calculations. The corresponding number of skeletal bonding electrons, 14, is consistent with that predicted for a *closo*-octahedron.[18]

Scheme 3

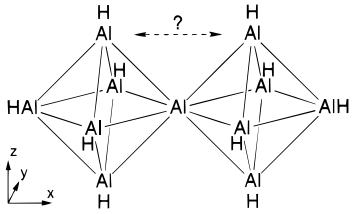

What happens to this magic electron count as the degree of cluster condensation through vertex-sharing increases? The assignment of formal charges in the alkaline-earth−transition-metal−aluminum intermetallics (which we carried out above) leads to approximately nine cluster bonding electrons per aluminum octahedron. Evidently, the optimal cluster electron count is reduced due to condensation through vertex-sharing. We will try to understand this phenomenon below.

Note that there are two modes of vertex-sharing in the aluminum substructure in Figure 1: "linear" along the *c* axis and somewhat bent or kinked in the *ab* plane. We concentrate on the effects of linear vertex-sharing for two reasons: the bent mode of vertex-sharing within the *ab* plane is not very different from linear and, also, bonding in the linear case is much easier to understand. Therefore, the following sections address the effect of linear vertex sharing on the optimal electron count for octahedral aluminum clusters in several model cases: a cluster dimer, a one-dimensional chain of clusters, a two-dimensional net, and a three-dimensional cubic network of clusters.

An $Al_{11}H_{10}$ Dimer

The first logical step in studying the effect of vertex-sharing on cluster bonding is to consider a dimer of two Al_6 H_6 octahedra, $Al_{11}H_{10}$ (Scheme 3).

The electronic structure of a similar dimer, only with boron atoms instead of the aluminum ones, has been discussed by Albright and Burdett.[22] It turns out that interactions between unshared atoms from different octahedra (indicated by a question mark in Scheme 3) are crucial in determining the optimal electron count for the cluster dimer. To understand this, we take still another step back and consider bonding in a square planar Al_4H_4. This fragment is important to our analysis, because it can be viewed as a building block in the $Al_{11}H_{10}$ dimer (AlH + Al_4H_4 + Al + Al_4H_4 + AlH), in the one-dimensional chain of clusters (... + Al_4H_4 + Al + Al_4H_4 + Al + ...), which will be considered shortly, and, of course, in Al_6H_6 itself (AlH + Al_4H_4 +AlH).

Square planar Al_4H_4 is related to a much better known molecule, cyclobutadiene (C_4H_4). The molecular orbitals of the latter, especially its π system, have been discussed thoroughly in many textbooks, so we simply present the Al_4H_4 version of them without much discussion. Figure 3 (center) depicts these molecular orbitals, separated into the following sets: four Al−H σ-bonding and four Al−H σ-antibonding orbitals (not shown); four Al−Al σ-bonding and four Al−Al σ-antibonding orbitals (also not shown); four aluminum-centered π orbitals. Figure 3 also shows how the orbitals of the Al_4H_4 fragment can be used to construct the orbitals of the Al_5H_5 square pyramidal fragment and Al_6H_6 cluster. These two constructions have also been presented elsewhere, for instance, by Albright and Burdett.[23] The optimal electron counts for both Al_5H_5 and Al_6H_6 are 14

(22) Albright, T. A.; Burdett, J. K. *Problems in Molecular Orbital Theory*; Oxford University Press: New York, 1992; problem 4.28, pp 111, 147.

(23) Albright, T. A.; Burdett, J. K. *Problems in Molecular Orbital Theory*; Oxford University Press: New York, 1992; problem 4.25, pp 109, 142.

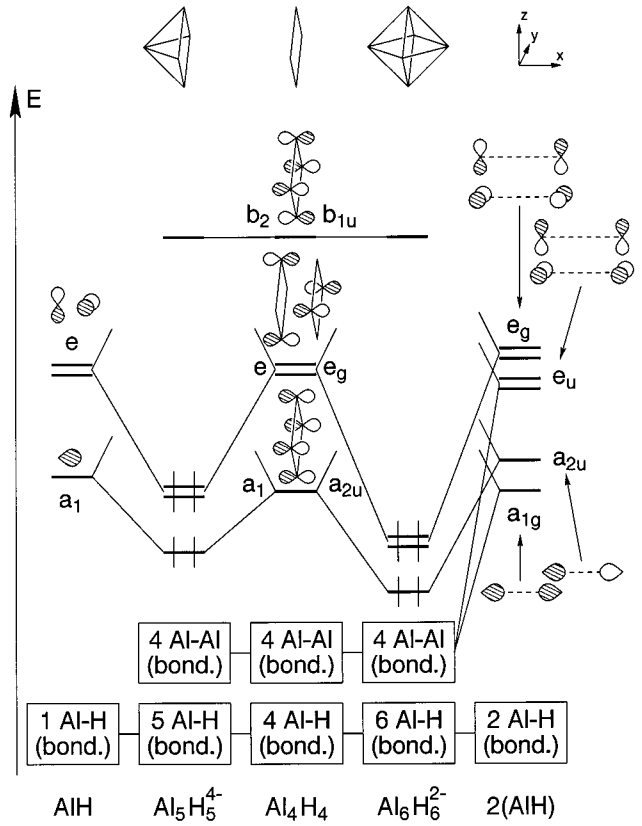

Figure 3. Qualitative interaction diagrams for $Al_5H_5^{4-}$ (left, orbitals are labeled according to C_{4v} symmetry) and $Al_6H_6^{2-}$ (right, orbitals are labeled according to D_{4h} symmetry) clusters using square planar Al_4H_4 and AlH as fragments. The four Al−Al σ-bonding orbitals of the Al_4H_4 fragment and their derivatives in $Al_5H_5^{4-}$ and $Al_6H_6^{2-}$, as well as the Al−H bonding orbitals, are shown schematically as separate blocks.

cluster electrons in each (in the four Al−Al bonding orbitals "boxed", and in the three other cluster bonding orbitals), again consistent with the *nido*- or *closo*-octahedral count. The seven filled Al−Al bonding orbitals of $Al_6H_6^{2-}$ in Figure 3 are, of course, identical to those in Figure 2.

Now we use the frontier orbitals of the $Al_5H_5^{4-}$ fragment, which are based on the π orbitals of the square planar Al_4H_4 unit, to describe the bonding in the cluster dimer, $Al_{11}H_{10}^{5-}$. Figure 4 depicts the interaction of two $Al_5H_5^{4-}$ fragments with an Al^{3+} ion. Note that in the "dimer" there are 28 electrons in cluster bonding orbitals, which is just two times 14 electrons, the optimal electron count for an isolated cluster. This is the main conclusion for such a cluster dimer.[18,22] However, as Albright and Burdett pointed out,[22] if the intercluster interactions (marked by a question mark in Scheme 3; in the model in question the distance is 4.09 Å) are sufficiently strong, the e_g level (HOMO) of the cluster dimer is substantially destabilized; this orbital is antibonding between the octahedra (see top left orbitals in Figure 4). This may favor oxidation of the $Al_{11}H_{10}^{5-}$ cluster by four electrons, reducing the number of cluster bonding electrons to 24, only 12 per cluster.

Up to now our considerations have been only qualitative. Figures 5 and 6 present the actual interaction diagrams for the formation of $Al_5H_5^{4-}$, $Al_6H_6^{2-}$, and $Al_{11}H_{10}^{5-}$. The bonding picture presented in Figures 3 and 4 is confirmed. It is apparent from Figure 6 that the HOMO of the cluster dimer (e_g) is indeed pushed up in energy due to the antibonding interaction between the clusters. At the same time the e_u orbitals, already bonding between and within the clusters, participate in bonding to the

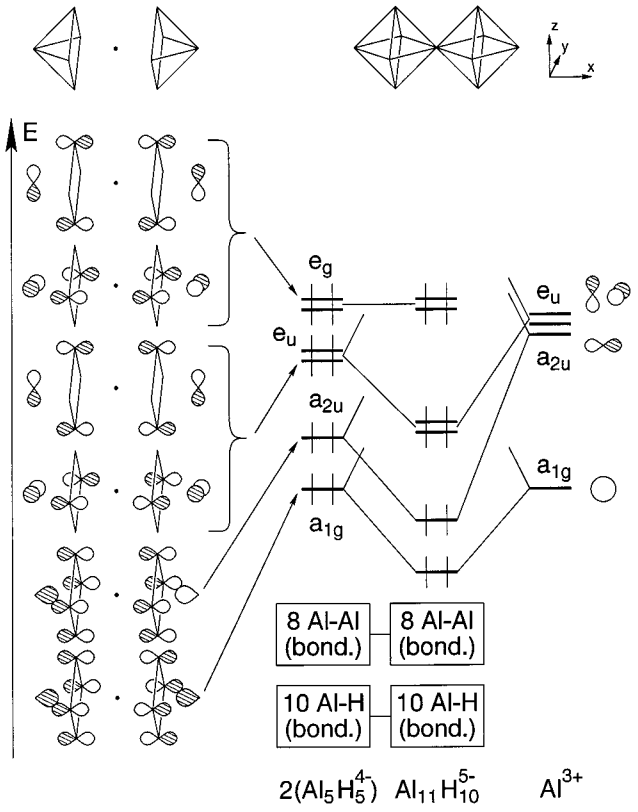

Figure 4. Qualitative interaction diagram for the $Al_{11}H_{10}^{5-}$ cluster dimer of D_{4h} symmetry built from two $Al_5H_5^{4-}$ fragments and an Al^{3+} ion. Al−Al σ-bonding orbitals of the Al_4H_4 fragments and the Al−H bonding orbitals are shown schematically as separate blocks.

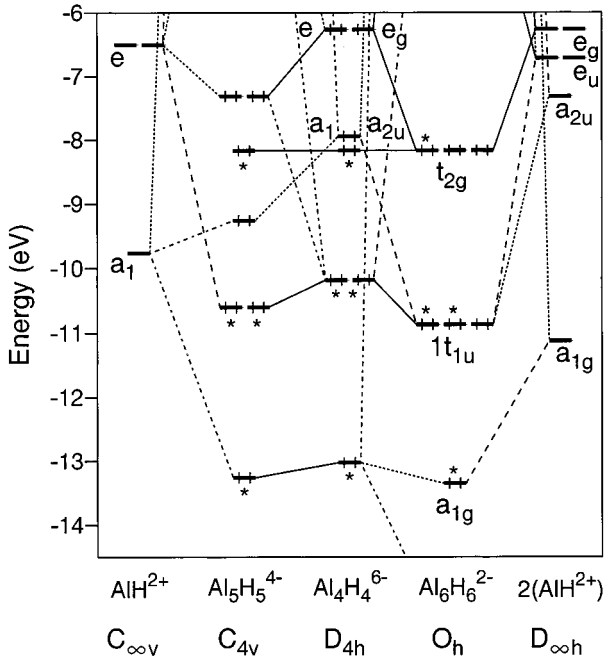

Figure 5. Computed interaction diagrams for the $Al_5H_5^{4-}$ and $Al_6H_6^{2-}$ clusters from the $Al_4H_4^{6-}$ fragment. Compare with Figure 3. Asterisks mark the Al−Al bonding orbitals shown grouped in blocks in Figure 3. The four Al−H bonding orbitals lie below −14.5 eV.

central aluminum atom and are lowered in energy. This creates a sizable 1.6 eV gap between HOMO and HOMO−1, suggesting that the cluster dimer might be oxidized by four electrons to a stable $Al_{11}H_{10}^{1-}$ with 12 bonding electrons per aluminum octahedron.

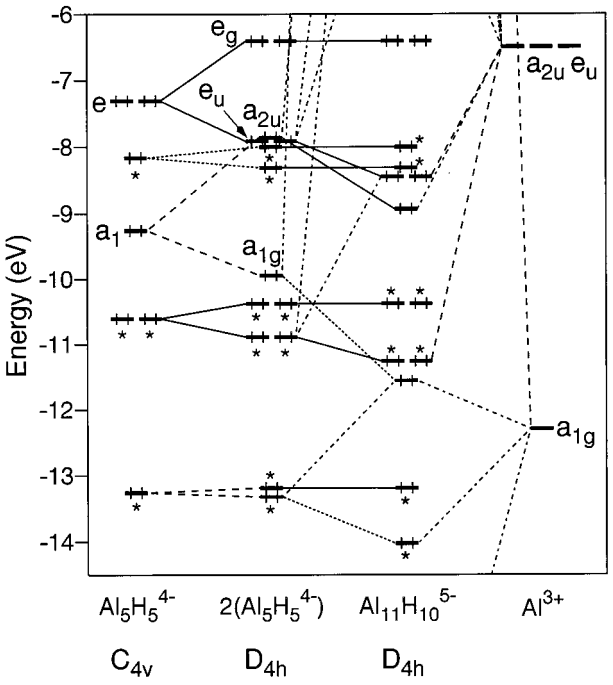

Figure 6. Computed interaction diagram for forming the $Al_{11}H_{10}^{5-}$ cluster dimer from two $Al_5H_5^{4-}$ fragments and an Al^{3+} ion. Compare with Figure 4. Asterisks mark the Al−Al bonding orbitals shown grouped in blocks in Figure 4. The Al−H bonding orbitals lie below −14.5 eV.

The intercluster Al−Al interactions are important in our calculations because the aluminum wave functions are rather diffuse: the intercluster Al3p−Al3p σ-type overlap at the relevant distance (4.09 Å) is 0.194, really quite substantial compared to an overlap of 0.377 for the nearest neighbor contact of 2.89 Å.

Here it is worth mentioning a recently synthesized Cs_6Ge_8Zn[24] phase: this Zintl-type compound contains isolated Ge_8Zn^{6-} clusters, which may be described as two vertex-sharing Ge_4Zn trigonal bipyramids (with the Zn vertex shared). There are 24 electrons available for cluster bonding, exactly twice 12—the magic number for a *closo*-trigonal bipyramidal cluster. The Ge−Ge contacts between the trigonal bipyramids are rather long because the shared vertex is apical in both Ge_4Zn units. It is not surprising then that the magic electron count per cluster is not altered by vertex sharing in this example.

A One-Dimensional Linear Chain of Vertex-Sharing Clusters

Having established the effect of vertex sharing on the electronic structure of the $Al_{11}H_{10}$ cluster dimer, we move on to an infinite system, a linear one-dimensional chain of vertex-sharing octahedral aluminum clusters (Scheme 4).

What electron count maximizes Al−Al bonding for such a chain? First, we construct a qualitative interaction diagram for the chain using orbitals of the square planar Al_4H_4 building block and isolated aluminum atoms. This interaction diagram is similar to that for Al_5H_5, only now we need to take into account translational symmetry. Figure 7 presents the important orbital interactions at two special points in the Brillouin zone: Γ (where the wave functions have the same phase in neighboring unit cells) and X (wave functions have the opposite phases in neighboring unit cells).[9] At the X point, seven bands are Al−Al bonding; we expect these bands to be filled with 14 electrons.

(24) Queneau, V.; Sevov, S. C. *J. Am. Chem. Soc.* **1997**, *119*, 8109.

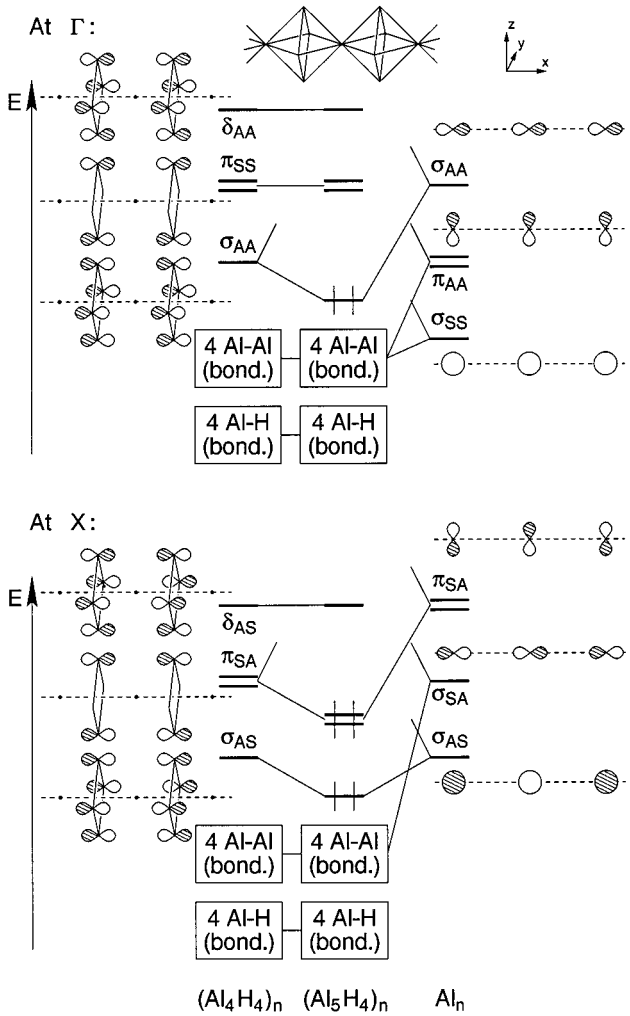

Figure 7. Qualitative interaction diagram for the $^1_\infty[Al_5H_4]$ chain at the Γ and X points in the Brillouin zone. The four Al−Al σ-bonding orbitals of the Al_4H_4 fragment, as well as the Al−H bonding orbitals, are shown schematically as separate blocks. The crystal orbitals are labeled according to the pseudo-cylindrical symmetry of the chain and with respect to two inversion centers: one in the center of each Al_4H_4 fragment and the other centered on bridging Al. Only the clearly bonding levels are shown filled; the actual position of the Fermi level is discussed in the text and Figure 8.

Scheme 4

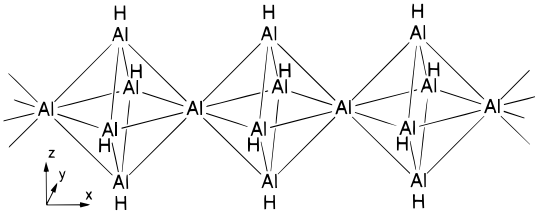

At the Γ point, however, the two π_{SS} bands are substantially Al−Al antibonding between the neighboring Al_4H_4 fragments. Remembering that such interaction was quite strong in the $Al_{11}H_{10}$ cluster dimer and realizing that now these interactions are approximately twice as strong in the chain (each Al_4H_4 fragment in the chain interacts in antibonding fashion with *two* neighboring fragments, as opposed to *one* in $Al_{11}H_{10}$), we expect these two bands to be unoccupied. Thus, there should be only five Al−Al bonding bands at Γ filled with 10 electrons. From these considerations, Al−Al bonding in the $^1_\infty[Al_5H_4]$ chain should be maximized when there are between 10 and 14

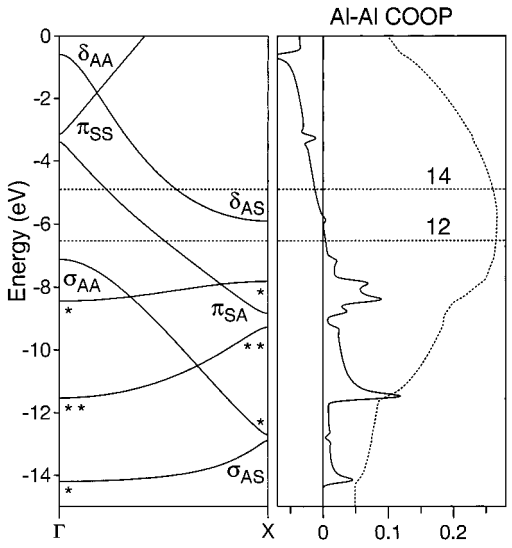

Figure 8. Computed band structure for a linear $^1_\infty[Al_5H_4]$ chain (left) and the average COOP for the nearest-neighbor and next-nearest-neighbor Al−Al contacts (right, the integration curve is shown by a dashed line). The two Fermi levels correspond to 14 and 12 cluster electrons. The crystal orbitals at Γ and X are assigned symmetry labels according to Figure 7, asterisks mark the Al−Al bonding states shown in Figure 7 grouped in a block. The Al−H bonding bands lie below −15 eV.

Scheme 5

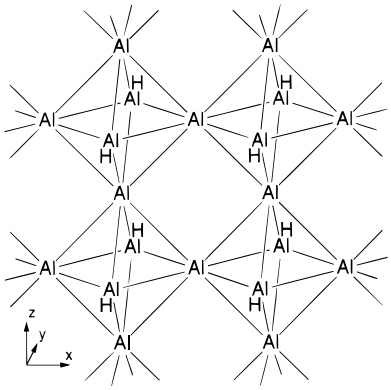

electrons in the unit cell (or 10−14 per aluminum octahedron, since there is one octahedron per unit cell).

The computed band structure for the chain and the crystal orbital overlap population (COOP,[9] a bond strength index) plot, averaged over the nearest-neighbor and next-nearest-neighbor Al−Al contacts are shown in Figure 8. The δ_{AS} band at X is lower in energy than the π_{SS} band at Γ. The δ_{AS} band at X then would be filled if we were to put 14 cluster electrons per unit cell in the chain; this band is also Al−Al antibonding, and thus, the 14-electron cluster count is unfavorable. As a result the 14-electron Fermi level cuts both the $\pi_{SS}-\pi_{AS}$ and $\delta_{AA}-\delta_{AS}$ band. The COOP integration curve reaches its maximum at a little over 12 electrons per unit cell, indicating that this is the optimal cluster electron count for the chain.

A Two-Dimensional Square Sheet of Vertex-Sharing Clusters

We have also studied the electronic structure of a two-dimensional square sheet of octahedral aluminum clusters (Scheme 5), although we do not give the details of the calculations here. The main conclusion of this investigation is that the optimal electron count for the aluminum clusters is again

Scheme 6

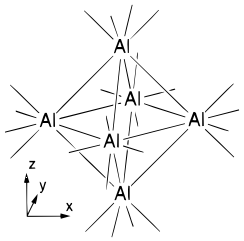

reduced from the 14 electrons. We find through COOP analysis that in the two-dimensional sheet the Al−Al bonding for 10 cluster electrons is stronger than that for 12 or 14 cluster electrons.

At this point it may be appropriate to introduce a structure that is actually related to our model. This is the $CeMg_2Si_2$[25] structure, which has a similar square two-dimensional network of vertex-sharing manganese−silicon octahedral clusters, with the silicon atoms taking place of the AlH units in Scheme 5 and Mg atoms shared between the clusters. The Si atoms are further linked between such Mg_2Si_2 layers by formally single Si−Si bonds. Assuming a $Ce^{4+}(Mg_2Si_2)^{4-}$ electron count, there are 16 valence electrons per octahedral cluster, two of which are in the Si−Si interlayer bond. The other 14 electrons are responsible for intracluster bonding, according to the analysis given by Zheng and Hoffmann.[26] However, only 10 electrons per octahedron occupy cluster bonding levels, while the other four electrons fill essentially nonbonding states. The Mg/Si clusters in $CeMg_2Si_2$ are far from being regular octahedra: they are strongly compressed in the direction perpendicular to the plane of the layers as evidenced by a large difference between the shorter intracluster Si−Si distances (3.19 Å, analogous to the AlH−AlH contacts along *y* in Scheme 5) and longer intercluster ones (4.25 Å, analogous to AlH−AlH contacts along *x* and *z* in Scheme 5). It is the latter longer contacts that could contribute, but because of their length do not do so, to the Si−Si antibonding nature of the actually nonbonding states. In our model $^2_\infty[Al_4H_2]$ the two corresponding Al−Al distances are both equal to 4.09 Å.

A Three-Dimensional Cubic Network of Vertex-Sharing Clusters

Now we turn our attention to another model system, a cubic $^3_\infty[Al_3]$ network of maximally vertex-sharing aluminum octahedra, with all vertices shared and no hydrogens left, schematically indicated by Scheme 6. In the process we return to a high-symmetry cubic group situation, as we had for molecular $Al_6H_6^{2-}$.

We again focus on the crystal orbitals of the system at the special points in the Brillouin zone. With one aluminum octahedron per unit cell of the cubic network, the vectors connecting the opposite vertices are also the lattice vectors. The special points are then as follows: Γ, with no change in phases along all three (*x*, *y*, and *z*) directions; X, with a change of phase only along the *x* axis; M, with a change of phase along both the *x* and *y* axes; R, with phases changing along all three directions.

Figure 9 shows schematically the crystal orbitals for the seven lower bands of the cubic network at the four special points. Note that the lower four bands at each special point are bonding with respect to nearest neighbor Al−Al contacts, while the other

(25) Zmii, O. F.; Gladyshevskii, E. I. *Sov. Phys. Crystallogr. Engl. Transl.* **1971**, *15*, 817.
(26) Zheng, C.; Hoffmann, R. *Z. Naturforsch.* **1986**, *41b*, 292.

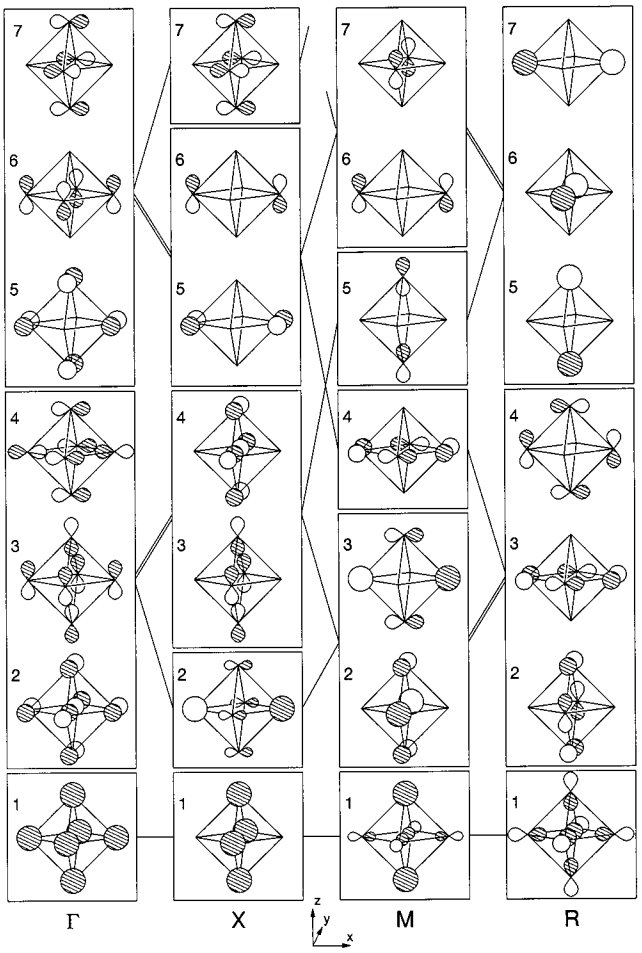

Figure 9. The lower seven crystal orbitals for the three-dimensional cubic net of vertex-sharing aluminum octahedra at Γ, X, M, and R.

three bands (bands 5−7) are Al−Al antibonding for nearest-neighbor or next-nearest-neighbor contacts. This suggests that, instead of having 14 electrons per cluster (which means 14 electrons per unit cell), the system may be able to accommodate only eight electrons in order to maximize Al−Al bonding.

The computed band structure for such a cubic network and the average Al−Al COOP curve for nearest-neighbor and next-nearest-neighbor contacts are shown in Figure 10, with the Fermi levels corresponding to 8, 10, 12, and 14 electrons per cluster marked. Clearly *eight* cluster electrons are optimal for Al−Al bonding in this network.

How can we understand qualitatively the decrease of the number of available bonding orbitals in the cubic network? The 14-cluster electron count was derived for an isolated cluster. The main difference between the molecular orbitals of such a cluster and the crystal orbitals of a cluster network is that in the latter there are additional restrictions imposed on the shape of the wave functions due to translational symmetry of the network. For example, at the Γ point the phase of any wave function must be the same on opposite aluminum atoms within the same octahedron. Thus, a t_{2g}-like orbital (see Figure 2) cannot participate in bonding at this special point. However, crystal orbitals resembling $1t_{1u}$ are allowed by translational symmetry; the bands 2−4 at Γ are derived from them with some admixture of $2t_{1u}$-like crystal orbitals. At the R point, however, t_{2g}-like crystal orbitals are allowed; they form bands 2−4 at that point. The t_{1u} local symmetry is now incompatible with the requirement of phase change along all three crystal axes. The a_{1g}-like crystal orbital is quite flexible in terms of satisfying

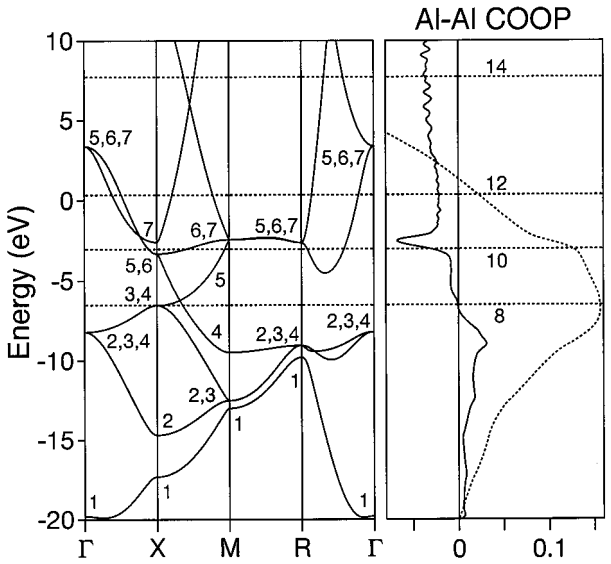

Figure 10. The computed band structure for the cubic network of vertex-sharing aluminum octahedra (left) and the average COOP plot for nearest-neighbor and next-nearest-neighbor Al−Al contacts. The COOP integration curve is shown as a dashed line. The Fermi levels are shown for 8, 10, 12, and 14 electrons per aluminum cluster. The bands are numbered according to Figure 9.

translational symmetry—it can be formed of pure p or pure s contributions, depending on the position of the crystal orbital in the Brillouin zone.

Thus, the presence of translational symmetry in the cubic network makes it impossible for seven Al−Al bonding crystal orbitals to exist at each special (or general) point of the Brillouin zone. The 14-electron rule is no longer valid. Instead, only four Al−Al bonding bands are present throughout the reciprocal space.

Incidentally, the fifth, the sixth, and the seventh bands, which "take the place" of the Al−Al bonding bands not allowed by translational symmetry, are typically antibonding with respect to next-nearest-neighbor Al−Al contacts, much like the e_g HOMO of $Al_{11}H_{10}^{5-}$ and the π_{SS} band at Γ of the $^{1}_{\infty}[Al_5H_4]$ chain (these rather long-range Al−Al antibonding interactions are also responsible for lowering the optimal cluster electron count in the square $^{2}_{\infty}[Al_4H_2]$ sheet).

Again we can relate the model $^{3}_{\infty}[Al_3]$ network to experimentally characterized compounds. Several rare earths form 1:3 intermetallics with aluminum. These compounds crystallize in the Ni_3Sn, $BaPb_3$, $TiNi_3$, $HoAl_3$, and Cu_3Au structure types[27,28] (the structure types are arranged according to the increasing cubic character based on the relative stacking of close-packed layers, with Ni_3Sn being purely hexagonal and Cu_3Au being purely cubic). The aluminum atoms of those rare earth aluminides which crystallize in the Cu_3Au structure type form exactly the cubic $^{3}_{\infty}[Al_3]$ network. We note that the $LnAl_3$ stoichiometry (Ln = lanthanide), together with lanthanides being more electropositive than aluminum, places 9−12 electrons per aluminum cluster into the aluminum network of the cubic rare-earth trialuminides. Correspondingly, the nearest neighbor Al−Al contacts in these compounds are elongated

(27) van Vucht, J. H. N.; Buschow, K. H. J. *J. Less-Common Met.* **1965**, *10*, 98.
(28) Cannon, J. F.; Hall, H. T. *J. Less-Common Met.* **1975**, *40*, 313.

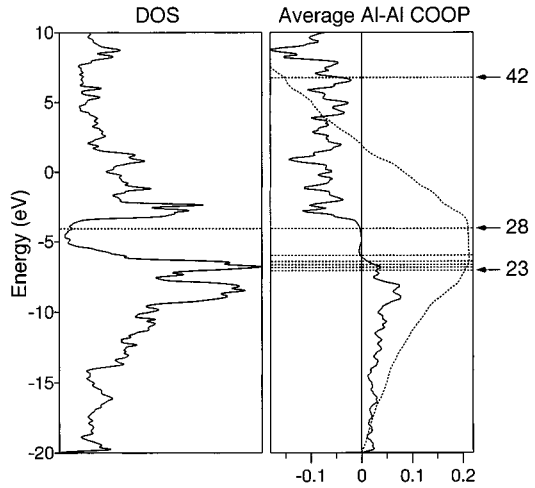

Figure 11. The computed density of states (DOS, left) for the hexagonal network of vertex-sharing aluminum octahedra as in Figure 1. The average Al−Al COOP curve (solid line) and its integration (dashed line) for the same system (right). The Fermi levels are shown for 23−28 and 42 electrons per unit cell ($7^2/_3 - 9^1/_3$ and 14 electrons per octahedron).

compared to 2.89 Å observed in the $BaFe_2Al_9$-type compounds (3.00 Å in $DyAl_3$, 2.99 Å in $HoAl_3$, 2.98 Å in $ErAl_3$, 2.97 Å in $TmAl_3$ and $YbAl_3$, 2.96 Å in $LuAl_3$, and 2.90 Å in $ScAl_3$) because Al−Al antibonding levels are partially filled. Interestingly, when a $LnAl_3$ compound can be obtained in several structure types, the cubic modification (Cu_3Au-type) is found to be less stable; it is typically obtained under high-pressure conditions. It is not clear, however, whether filling of the Al−Al antibonding states is responsible for this effect: other explanations have been proposed as well.[28]

A Three-Dimensional Hexagonal Network of Vertex-Sharing Clusters

Now we turn our attention to the hexagonal network of vertex-sharing aluminum clusters shown in Figure 1, the Al sublattice of the AeM_2Al_9 compounds which were the starting point for our discussion. In view of the preceding analysis, we expect the Al−Al bonding to be at its maximum for about eight electrons per octahedron. As the orbital analysis of such a network is quite laborious (this is why we analyzed similar, but more symmetrical systems first), we simply present the results of our calculations in Figure 11. The density of states (DOS) and the COOP plots are shown. The COOP values were computed as an average over all relatively short Al−Al contacts, including both the nearest-neighbor Al−Al contacts within the octahedra and the next-nearest-neighbor ones.

There are several observations to be made. First of all, the 14-cluster electron count (42 electrons per unit cell) is definitely out of the question, because it corresponds to a physically unreasonable position of the Fermi level and net Al−Al antibonding. Next we note that the DOS conveniently develops a dip, almost a gap, at −5 eV (there is no actual band gap, however). The COOP curve indicates that the states below this energy are on average Al−Al bonding, while the higher-lying states are Al−Al antibonding. For the Fermi level to be in the dip of the DOS curve, approximately 28 electrons per unit cell, which has three clusters, are needed. This corresponds to the maximum of Al−Al bonding; there are $9^1/_3$ electrons per aluminum cluster for such a count. There is actually a plateau in the COOP integration curve in that region, which suggests that the Al−Al bonding can remain close to optimal for a range of electron counts near that value. The corresponding positions of the Fermi level are shown in Figure 11 for 23−28 electrons per unit cell ($7^2/_3 - 9^1/_3$ cluster electrons). This is in agreement with both our expectation of approximately eight cluster electrons, and the $8^1/_3 - 9^2/_3$ cluster electron counts obtained from assigning formal charges to alkaline-earth and transition-metal atoms earlier in this study.

There are three different types of Al−Al bonds in this network. Bonds of the first two types form hexagons and triangles in the *ab* plane, as can be seen in Figure 1a. Bonds of the third type involve aluminum atoms shared between octahedra along the *c* axis. The computed COOP values for these bond types are quite different: at $9^1/_3$ cluster electrons (28 per unit cell) these values are 0.505, 0.282, and 0.376. While there is a large difference between the bonds forming hexagons and triangles in the *ab* plane, the average of the two corresponding COOP values (0.394) is rather close to that for the bonds of the third type. When a calculation on the bulk $BaFe_2Al_9$ structure is carried out, the COOP values of 0.452, 0.220, and 0.281 (the average of the first two is 0.336) are obtained for the same contacts.

Such a large difference in the COOP values for the different Al−Al bonds in the *ab* plane suggests that a distortion is to be expected, such that the hexagonal channels of the network become narrower and the trigonal channels become wider. The atoms filling the channels may alter the situation somewhat: we compute the Fe−Al interactions (in the trigonal channels) to be substantially bonding, while the Ba−Al interactions (in the hexagonal channels) are essentially nonbonding. This finding could be certainly used to argue that the Fe−Al interactions are what prevents the triangular channels from expanding relative to the hexagonal ones. But the extended Hückel method is not a reliable tool for a quantitative comparison of the Al−Al, Fe−Al, and Ba−Al bond strengths. Given the fact that the Al−Al bonds around the hexagonal channels are computed to be approximately twice as strong as the Al−Al bonds around the trigonal channels, we believe that this structural issue is worth studying experimentally by refining the AeM_2Al_9 structures in order to obtain more reliable values for the distinct Al−Al bond lengths.

Conclusions

Several simple model systems were analyzed to study the effect of vertex-sharing between aluminum octahedral clusters on the electron count optimal for Al−Al bonding. An isolated Al_6H_6 cluster, a linear cluster dimer $Al_{11}H_{10}$, a linear $^1_\infty[Al_5H_4]$ chain, a square $^2_\infty[Al_4H_2]$ sheet, and a cubic $^3_\infty[Al_3]$ network have been considered. The optimal cluster electron count is reduced from 14 electrons for the isolated cluster. The Al−Al bonding is maximized for 12 cluster electrons per octahedron in $Al_{11}H_{10}$, for somewhat more than 12 cluster electrons in the linear $^1_\infty[Al_5H_4]$ chain, for 10 cluster electrons in the square $^2_\infty[Al_4H_2]$ sheet, and for eight cluster electrons in the cubic $[Al_3]$ network.

This effect can be linked to two factors. First of all, the number of available Al−Al bonding orbitals per cluster is reduced, due to restrictions imposed by the translational symmetry of the lattice (this was shown to be the case for the cubic network). Second, the orbitals lying immediately above the Al−Al bonding states in energy are likely to be unoccupied because they are mostly next-nearest-neighbor Al−Al antibonding.

The results of our analysis are not restricted to aluminum. Since the arguments used are based to a large extent on the

topology of the network, it is not surprising that our model calculations for analogous octahedral phosphorus clusters (isolated and condensed into a $^3_\infty[P_3]$ network) also suggest a similar reduction of the magic cluster electron count. Notably the crystal orbitals of the $^3_\infty[P_3]$ network are nearly identical to those of the $^3_\infty[Al_3]$ system.

Reasoning by analogy and on the basis of our calculations, we understand why the hexagonal network of vertex-sharing aluminum clusters in AeM_2Al_9 (Ae = Ca−Sr; M = Fe−Ni) and in $CaNiAl_9$ exists for $8^1/_3 - 9^2/_3$ cluster electron counts. In these systems, the Fermi level lies near a gaplike dip in the DOS curve and separates the Al−Al bonding states from the Al−Al antibonding ones.

Acknowledgment. Thanks are due to our research group at Cornell University for comments and suggestions. This work was supported by the National Science Foundation through Research Grant CHE 94-08455 and by the S. T. Olin Foundation through a graduate fellowship.

Appendix: Alkaline-Earth and Transition-Metal Bonding

We describe briefly the bonding at the alkaline-earth and transition-metal atoms in the AeM_2Al_9 intermetallics, using $BaFe_2Al_9$ as an example. Ba atoms fill the hexagonal channels of the aluminum network, as mentioned previously. Specifically, each Ba center is surrounded by a hexagonal prism of Al atoms with the Ba−Al distance of 3.54 Å, with six longer Ba−Al contacts of 4.02 Å. Such distances are typical for the Ba−Al interactions: in $BaAl_4$,[29] for example, the Ba−Al bond lengths are 3.59 and 3.47 Å.

Aluminum atoms form trigonal prisms around the Fe atoms; these prisms are also capped by Al on rectangular faces. The Fe−Al distance for the three capping aluminum atoms is 2.32 Å; the other six Fe−Al bonds are 2.58 Å long. We may describe the Fe as nine-coordinate, in a tricapped trigonal prism geometry. A typical Fe−Al distance in intermetallics is 2.51 Å (as in $FeAl$[30]), which is very similar to the bond lengths of 2.510 Å[31] and 2.456 Å[32] for single Fe−Al bonds in organometallic compounds. Therefore, the shorter Fe−Al contact in $BaFe_2Al_9$ is certainly indicative of strong Fe−Al interaction.

We carried out calculations on $BaFe_2Al_9$ in the experimentally observed structure (with Al−Al distances of 2.93 Å in the *ab* plane and 2.85 Å for the other Al−Al bond type). The results are generally predictable; the only surprise is that the Fe 3d block of orbitals remains undispersed in energy (and therefore completely filled, as suggested earlier in this study). We link this to the mutually canceling effects of trigonal planar and trigonal prismatic coordination on the crystal field orbital splitting at the iron center. Fe 4s and 4p orbitals remain mostly unoccupied in the computed bulk structure, corresponding to the $3d^{10}4s^04p^0$ formalism.

JA974132C

(29) Andress, K. R.; Alberti, E. *Z. Metallkd.* **1935**, *27*, 126.
(30) Sidorenko, F. A.; Kotov, A. P.; Zelenin, L. P.; Gel'd, P. V. *Phys. Met. Metallogr. Engl. Transl.* **1973**, *35*, 209.
(31) Burlitch, J. M.; Leonowicz, M. E.; Petersen, R. B.; Hughes, R. E. *Inorg. Chem.* **1979**, *18*, 1097.
(32) Fischer, R. A.; Priermeier, T. *Organometallics* **1994**, *13*, 4306.